

On Measurements of the Water-Particle Velocity under Breaking Waves over the Horizontal Step in a Laboratory Tank

Takeo Nakagawa

Department of Mechanical System Engineering, Kanazawa Institute of Technology, Kanazawa, Japan

ABSTRACT

Three velocity components of water particles in spilling and plunging breakers, respectively, have been measured simultaneously by means of an elaborate flowmeter in a two-dimensional wave tank. This new flowmeter measures the flow drag on three tension threads, each recording a separate flow component. Subsequently, steady flow and unsteady flow, turbulent fluctuation and power-spectral density are discussed for understanding and modeling the surf zone in a laboratory.

INTRODUCTION

Much of what is visible of a breaking wave is the combination of air and surface tension in drops and bubbles, containing salt (Scott, 1975). Breaking waves are one of the permanent subjects that have attracted numerous researchers as well as artists. Excellent reviews on this subject can be found in Peregrine (1983) and Battjes (1988).

Offshore breaker types are either spilling or plunging. For a spilling breaker, the wave shape remains more or less symmetrical, while a plunging breaker is characterized by a steepening and overturning of the front face, and the formation of a jet that plunges into the water ahead of the wave. The breaking process of a spilling breaker is, however, essentially the same as that of a plunging breaker in the initial phases, except that for the former, the process is confined to a relatively small region near the top of the wave.

The progress of study on breaking waves has been greatly hampered by difficulties encountered in modeling the surf zone in a laboratory, and in measuring the water particle velocity. In the laboratory, water particle velocity in breaking waves has been measured by Morison and Crooke (1953), using neutrally buoyant particles. This study has shown that the greatest horizontal water particle velocity occurs when a wave breaks, and that there is a difference between the onshore and offshore velocities. Adeyemo (1970) has measured the velocity field near breakers with hydrogen bubbles and has discussed the asymmetry of wave profile and velocity. Nadaoka (1986) has recently measured water particle velocities in the *bore* region behind a periodic breaking wave over the slope in terms of a laser-Doppler velocimeter. It has been inferred by Nadaoka (1986) that the rotational part of the phase averaged velocity makes a substantial contribution to the averaged wave-induced fluxes of mass, momentum and energy. In the surf zone, the water particle velocities have been measured with instruments like acoustic flowmeters (Miller and Ziegler, 1964), electromagnetic flowmeters (Thornton, Galvin, Bub and Richardson, 1976), propellers (Walker, 1969), and dye tracer (Wood, 1973).

It may be evident that measurements using neutrally buoyant particles, hydrogen bubbles and dye tracers provide only the qualitative data. Acoustic and electromagnetic flowmeters have a

common disadvantage: a large bulk at the point of measurement. Small propellers are of low sensitivity and low accuracy. Laser-Doppler velocimeters could measure three velocity components of water particles concurrently. However, such delicate and expensive instruments may not withstand the harsh conditions normally encountered in the surf zone. Hot wires, which have been used extensively in wind-tunnel researches, are too sensitive to contamination by the inevitable impurities in the water and to variation in the ambient temperature.

The first purpose of this paper is, therefore, to demonstrate that three velocity components of water particles both in spilling and plunging breakers over the horizontal step on the bed of a two-dimensional laboratory wave tank can be determined concurrently by means of an elaborate flowmeter sensing the flow drag on the three tension threads, each measuring a separate flow component. It is considered that the present flowmeter, referred to as the tension-thread flowmeter, compensates for the deficiencies of existing flowmeters as mentioned above, for this new flowmeter has a great potential to be a simple and inexpensive means of measuring velocity in water, like hot-wire anemometry in air flows.

The second purpose is to elucidate how steady and unsteady flow, turbulent fluctuation, and power-spectral density depend on the distance from the breaking point. This paper will discuss mainly the results regarding the plunging breaker; those on the spilling breaker may appear elsewhere.

APPARATUS

A detailed description of the present apparatus has been given in the two earlier publications by the author (Nakagawa, 1983a, 1983b), so that it will be explained very briefly here. Fig. 1 shows a schematic diagram of the experiment. This has been conducted in a two-dimensional wave tank 0.7 m wide. The wave generator is a hybrid type of piston and flap. Fig. 2a shows a view of the tension-thread flowmeter. The flow velocity can be measured by the three cotton threads (1, 2 and 3), which record velocities in the x -, y -, and z -directions, respectively. One end of the thread is fixed rigidly to the head of the screw-rod of the clamped support assembly, while the other end is knotted at the free end of a cantilever, enclosed within the elastic support assembly, two cross-sections of which are depicted in Fig. 2b. Note that the cantilever is designed so as to deflect only normal to its plane.

The length and diameter of the cotton threads are of 55 mm and 0.1 mm, respectively. The material of the thread does not have to

Received March 2, 1990; revised manuscript received by the editors November 14, 1990.

KEY WORDS: Breaking wave, flowmeter, turbulence, water particle, velocity, power spectrum.

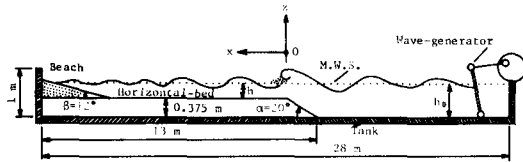


Fig. 1 Schematic diagram of the experiment

be cotton as long as the quality does not change during the measurement. Threads 1 and 3 are suspended in the same horizontal plane and parallel each other, where the distance between the two threads is 20 mm. On the one hand, thread 2 is in a horizontal plane at 15 mm below the plane including threads 1 and 3, but thread 2 is normal to threads 1 and 3. It is clear, therefore, that the velocity measured by the present flowmeter is an integrated mean velocity at a small space where the three threads are suspended. However, in the data analyses, the geometrical center of the three middle points of the threads is assumed to be the measuring point.

Calibrations of the flowmeter have been made in a tank filled with still water. The plane of the cantilever is carefully set normal to the longitudinal axis of the tank. The flowmeter is towed along the axis at a specified speed in the water; the output electrical signal is then recorded on the tape. In this way, the flowmeter has been calibrated in the 3.0-120 cm/s velocity range. This flowmeter seems to be superior in the dynamic response to any other flowmeter. That is, the forced-oscillation test in water shows that the natural frequency of the dynamic system of the flowmeter is approximately 100 Hz.

It is impossible to avoid completely some effects on the flow due to the rigs placed in it. These have been minimized, however, by the use of circular rods of small diameter (5 mm) for the frame, for example, and by adopting a design criterion such that each flow component is not disturbed by any rod, insofar as the flow is normal to the plane of the cantilever. Moreover, it may be clear that the measurement error in the flow velocity due to entrained air bubbles is proportional to the void ratio, so that the water particle velocity must be underestimated to some extent. It may be worth noting that the noise levels in the calibration tests are only several percents of the mean output electrical signal in the velocity range adopted for the measurement.

METHOD

Experiment

The measuring point in the wave tank is varied both in the longitudinal and vertical directions, but the transverse position is kept at the center. During the measurements of water particle velocities, water surface elevations have been recorded with two capacitance-type wave gauges simultaneously. Water surface elevations are measured at 1.0 m behind the wave generator, and the same longitudinal position as the water particle velocity is measured.

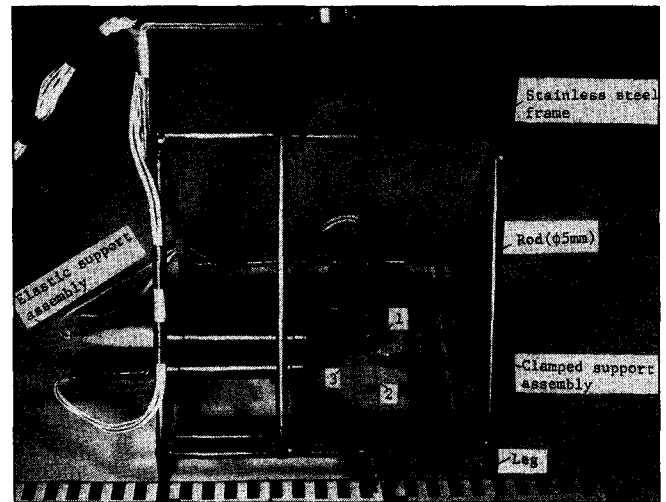


Fig. 2a Tension-thread flowmeter. One unit of the scale is 1 cm.

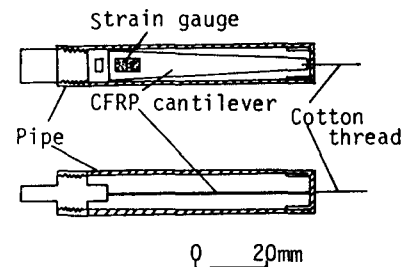


Fig. 2b Cross-sections of the elastic support assembly

However, it must be noted that the measurement of wave elevations using a capacitance-type wave gauge is limited when wave breaking is involved. This is due to the presence of trapped and/or entrained air and the multiple air/water interface in the case of a plunging wave.

Wave parameters in this study are summarized in Table 1, where the wavelength L is calculated from the dispersion relation of the small amplitude wave theory. Subscripts $\langle s \rangle$ and $\langle p \rangle$ denote spilling and plunging breakers respectively. Fig. 3 shows a photograph of a plunging breaker when the water jet from the wave crest has just broken. In the case of a spilling breaker, the measuring points range over 11 m in the longitudinal direction, and from 2 cm above the horizontal bed (or tank bed), to 2 cm below the wave trough in the vertical direction. Although trough elevation of the wave changes along the central axis of the tank, each measuring point is always set at 2 cm below wave trough. Intervals between the measuring points in the longitudinal and vertical directions are 10 cm and 3 cm, respectively. In case of a plunging breaker, the measuring points range over 9 m in the longitudinal

	At 1 m behind wave generator				At wave breaking point			
	Height [cm]	Period [s]	Depth [cm]	Wavelength [cm]	Height [cm]	Period [s]	Depth [cm]	Wavelength [cm]
Spilling breaker	$(H_s)_o$ 14.3	$(T_s)_o$ 1.5	$(h_s)_o$ 66.5	$(L_s)_o$ 307	H_s 14.7	T_s 1.5	h_s 29.8	L_s 264
Plunging breaker	$(H_p)_o$ 10.7	$(T_p)_o$ 1.4	$(h_p)_o$ 56.5	$(L_p)_o$ 265	H_p 13.3	T_p 1.4	h_p 19.5	L_p 186

Table 1 Wave parameters

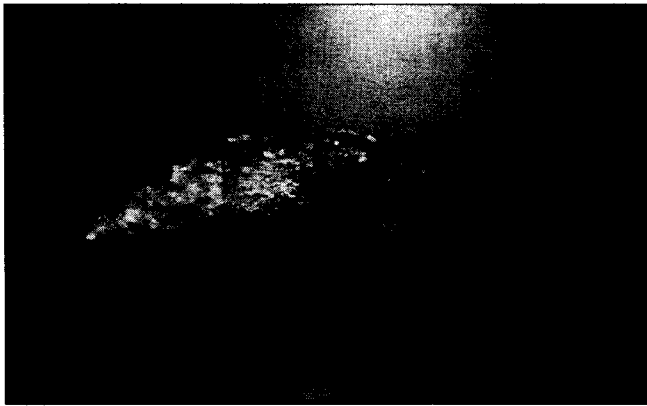


Fig. 3 The present plunging breaker. Wave direction is from right to left facing the wave.

direction, and from 2 cm above the horizontal bed, to 2 cm below the wave trough in the vertical direction. Intervals between the measuring points in the longitudinal and vertical directions are 10 cm and 2 cm, respectively. It may be worth noting here that no attempt was made to measure water particle velocities above the wave trough, although the present flowmeter has no limitation in doing that.

Data Analysis

The water particle velocities (u, v, w) are first separated into steady flows (U, V, W) and unsteady flows ($\hat{u}, \hat{v}, \hat{w}$). Unsteady flows are then divided into periodic flows ($\hat{u}, \hat{v}, \hat{w}$) and turbulent fluctuations (u', v', w'). The unsteady flows are also used to obtain the power-spectral densities.

Steady flow and unsteady flow. Steady flows are defined as the displaced distances of the water particle per wave period, or the mass transport velocities. Thus, unsteady flows may be obtained as $(\hat{u}, \hat{v}, \hat{w}) = (u-U, v-V, w-W)$.

Turbulent fluctuation. There is no established definition of the turbulent fluctuation of the water particle velocity in a breaking wave. It is evident, however, that once the periodic flows are ob-

tained by a certain way, the turbulent fluctuations can be given by $(u', v', w') = (\hat{u} - \hat{u}, \hat{v} - \hat{v}, \hat{w} - \hat{w})$.

The author (Nakagawa, 1983a) has therefore proposed a plausible method—the phase-average method—for separating periodic and turbulent components. With this method, a periodic flow component at each phase is defined as the arithmetic average of a number of the unsteady flow velocity component at the phase in several successive waves. Repetition of this procedure at each phase provides the periodic flows over the full 360° phase. In this analysis, five successive waves are used. Thus, one can obtain a turbulent fluctuation at each phase as the difference between the unsteady flow velocity component and the periodic flow velocity component.

Power-spectral density. The power-spectral density of unsteady flows is calculated by digital cosine transformation of the auto-correlation function (Blackman and Turkey, 1958), where the data numbers are 512; lag numbers, 200; and degrees of freedom, 5.

RESULTS AND DISCUSSION

In this section, wave height, steady flow, unsteady flow, turbulent fluctuation and power-spectral density will be presented and discussed, separately. However, before presenting and discussing these results, it may be essential to indicate how the wave breaking point is defined in this study: The wave breaking point for the spilling breaker is defined as the longitudinal position at which the wave height becomes maximum, whereas the wave breaking point for the plunging breaker is defined as the longitudinal position at which the wave front becomes vertical.

Wave height. Fig. 4 shows how wave heights for spilling and plunging breakers depend on the normalized distance from the breaking point, where H_s and H_p are wave heights for spilling and plunging breakers respectively, x the distance from the breaking point, L_s and L_p wavelengths for spilling and plunging breakers respectively, and subscript $\langle o \rangle$ denotes values at 1 m behind the wave generator. In the case of a spilling breaker, $H_s/(H_s)_o$ repeats the gradual increase and decrease while approaching the breaking point, and takes the maximum value of about 1.02 just before the breaking point. That is, the maximum wave height of the spilling

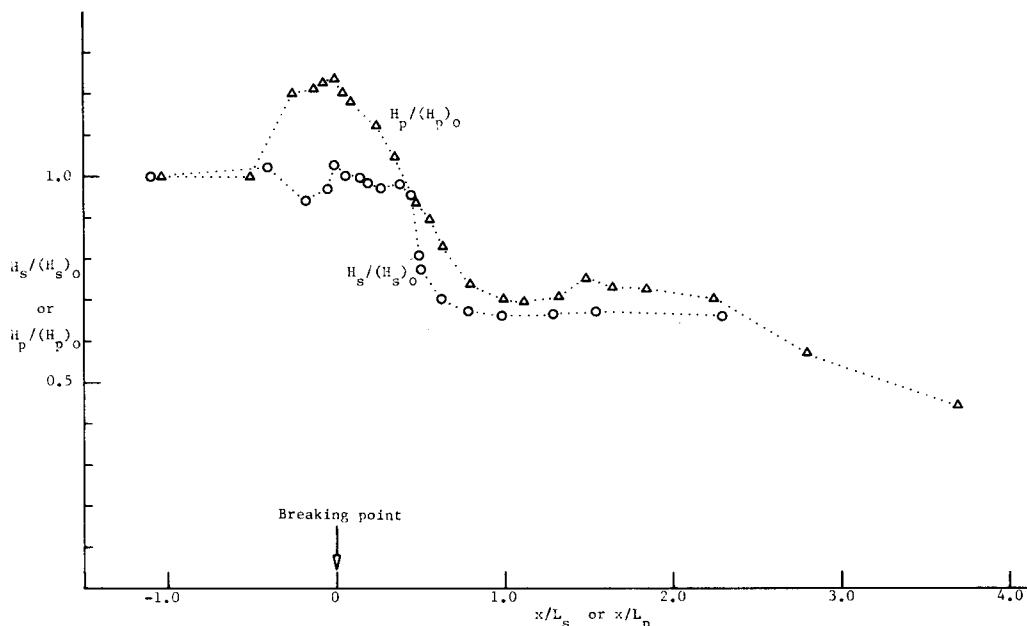


Fig. 4 Wave height H/H_o against distance x/L for spilling and plunging breakers, respectively.

breaker exceeds the original value only slightly. Behind that point, $H_s/(H_s)_o$ decreases slowly until $x/L_s \approx 0.5$. Then, $H_s/(H_s)_o$ decreases very rapidly with increasing x/L_s and becomes about 0.65 at $x/L_s = 1.0$. However, this value is kept almost constant until $x/L_s \approx 2.3$.

In the case of a plunging breaker, $H_p/(H_p)_o$ increases steeply while approaching the breaking point, and takes the maximum value of about 1.25 just before the breaking point. After the wave breaking, $H_p/(H_p)_o$ decreases exponentially with increasing x/L_p and becomes about 0.7 at $x/L_p = 1.0$. Then, $H_p/(H_p)_o$ increases gradually with increasing x/L_p and takes a moderate peak at $x/L_p \approx 1.3$. Behind this peak, $H_p/(H_p)_o$ decreases slowly with increasing x/L_p and becomes about 0.5 at $x/L_p \approx 3.7$.

These results are consistent with Svendsen, Madsen and Hansen (1978). They have reported that waves normally lose about 50% of their height after the breaking while traveling a distance less than 10 times the water depth at the breaking point.

Steady flow. In the case of a spilling breaker, the spatial distribution of the steady flows (U, V, W) in the vertical cross-section through the longitudinal central axis of the wave tank indicates that there is no definite locus along which the water mass is transported. On the other hand, in the case of a plunging breaker, it has been reported by the author (Nakagawa, 1983a) that near the water surface the water mass is transported from the breaking point to both onshore and offshore directions, while near the horizontal bed it is transported from the shore to the breaking point.

Unsteady flow. Fig. 5 shows time histories of the water surface elevation η and the unsteady flows ($\hat{u}, \hat{v}, \hat{w}$) at $x/L_p = -0.05$ (before the breaking point) and at 2 cm below the wave trough. At this position, η \hat{u} -correlation is quite large, and η \hat{v} -correlation and η \hat{w} -correlation are also evident. Through the wave shoaling process, wave profiles take on a cusp-like shape, but they maintain regularities. It is clear that there is a difference between the onshore and offshore velocities. That is, onshore velocity is greater than offshore.

Fig. 6 shows time histories of the water surface elevation η and the unsteady flows ($\hat{u}, \hat{v}, \hat{w}$) at $x/L_p = 0.16$ (after the breaking point) and at 2 cm below the wave trough. At this position, η \hat{u} -correlation is fairly large, but η \hat{v} -correlation becomes small, though η \hat{w} -correlation in this case is comparable to that in Fig. 5. Note that η -phase is almost identical to \hat{u} -phase, but it never coincides with \hat{v} -phase and \hat{w} -phase, respectively.

Figs. 7a, 7b and 7c show time histories of the water surface elevation η and the unsteady flows ($\hat{u}, \hat{v}, \hat{w}$) at $x/L_p = 0.6$ and at 2 cm below the wave trough (Fig. 7a), 6 cm above the horizontal bed (Fig. 7b), and 2 cm above the horizontal bed (Fig. 7c). These figures indicate that η \hat{u} -, η \hat{v} -, and η \hat{w} -correlations decrease while the measurement point approaches the horizontal bed, and at each depth η \hat{u} -correlation is largest, while η \hat{v} -correlation is smallest. It may be notable that \hat{v} highly fluctuates near the horizontal bed. This must be caused by the interaction of the water particle movement and the horizontal bed. Moreover, at this longitudinal position, not only the water surface elevation η , but also the unsteady flows ($\hat{u}, \hat{v}, \hat{w}$) oscillate in a random manner. It may be interesting to point out that in these time histories of the water surface elevation there exists a tiny bulge at each trough between the adjacent crests. That is, these bulges in the water surface elevation are impressed in the time histories of the unsteady flows.

Figs. 8a and 8b show time histories of the water surface elevation η and the unsteady flows ($\hat{u}, \hat{v}, \hat{w}$) at $x/L_p = 3.6$, and at 2 cm below the wave trough (Fig. 8a) and 2 cm above the horizontal bed (Fig. 8b). These figures show that η \hat{u} -, η \hat{v} -, and η \hat{w} -correlations at 2 cm below the wave trough are greater than those at 2

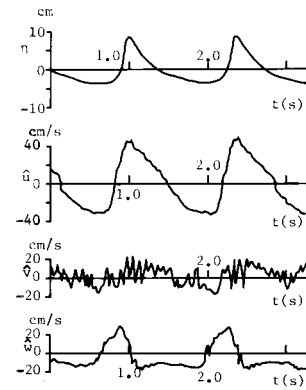


Fig. 5 Time histories of η , \hat{u} , \hat{v} , and \hat{w} at $x/L_p = -0.05$ and at 2 cm below the wave trough.

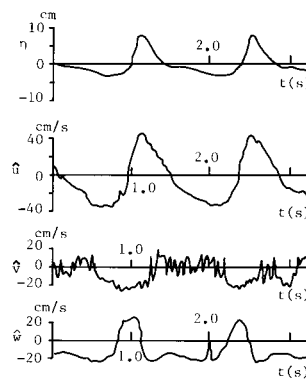


Fig. 6 Time histories of η , \hat{u} , \hat{v} , and \hat{w} at $x/L_p = 0.16$ and at 2 cm below the wave trough

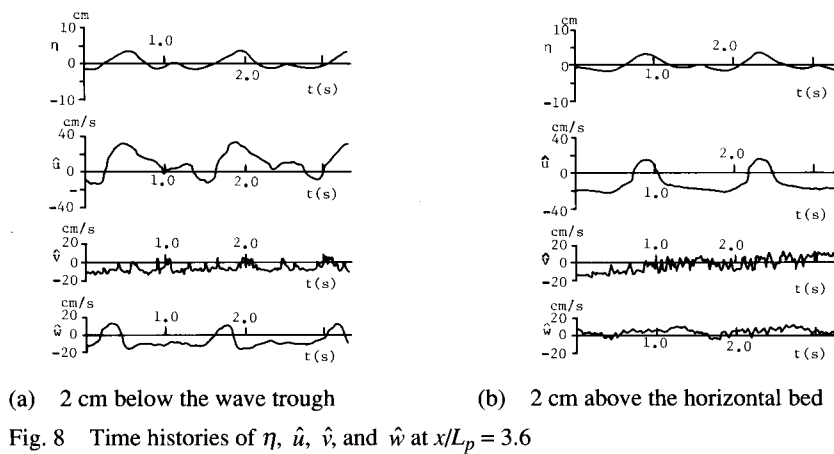
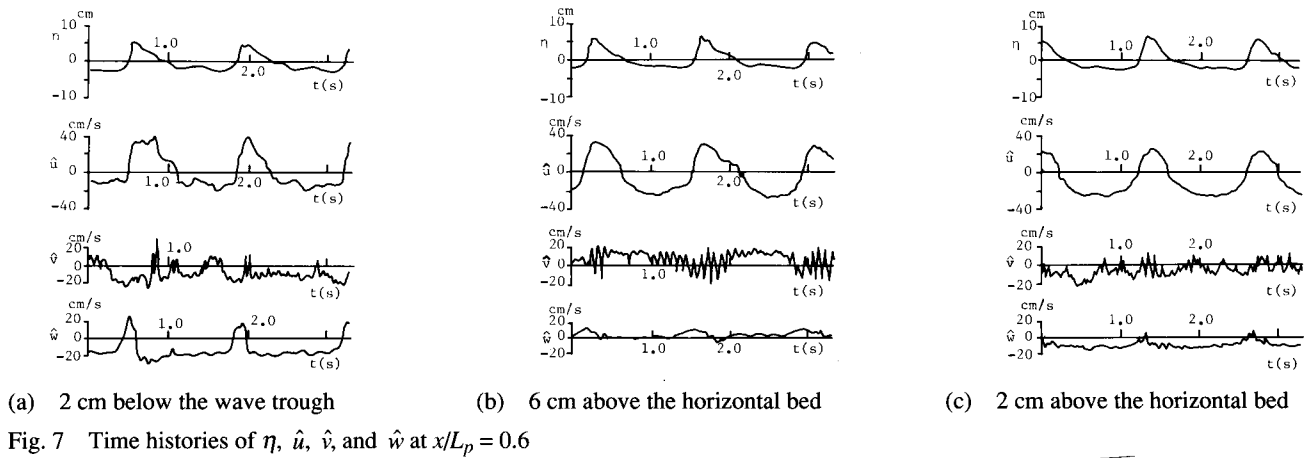
cm above the horizontal bed. Time histories of the water surface elevation and the unsteady flows become symmetrical again at this longitudinal position, while the bulge at each trough is more pronounced than that in Fig. 7.

Figs. 5-7 show that with increasing x/L_p , the difference between the onshore and offshore velocities increases, whereas the asymmetry of the wave profile decreases.

In this paper, the steady flows (U, V, W) are defined as displaced distances of the water particle per wave period, but in general they do not coincide with the displaced distances per unit time. In other words, the steady flow components may not be constant during the wave period. This may be the main reason why the mean values of unsteady flows in Figs. 5-7 are not zero.

Turbulent fluctuation. Fig. 9 shows how the turbulent fluctuations (u'_p, v'_p, w'_p) in the plunging breaker depend on the normalized distance x/L_p from the breaking point. The turbulent fluctuations have been determined by the phase-average method. The x -component u'_p increases with increasing x/L_p and takes the maximum value at $x/L_p \approx 0.7$. Behind this point, u'_p decreases rapidly with increasing x/L_p . Both the y -component v'_p and z -component w'_p exhibit similar dependency on x/L_p as u'_p . In the upstream of $x/L_p \approx 0.7$, u'_p and v'_p are smallest and largest, respectively, and in the sufficiently downstream their positions are reversed. However, near $x/L_p \approx 0.7$, u'_p is largest, while w'_p is smallest.

Power-spectral density. Figs. 10a, 10b, 10c and 10d show the power spectra of the water surface elevation η for the plunging breaker at $x/L_p = -0.05, 0.16, 0.6$ and 3.6 , respectively. It is seen that the potential energies of the wave at the fundamental fre-



quency f_0 and higher harmonic frequencies $f_1 - f_6$ are gradually transferred both to the higher and lower frequency ranges with increasing x/L_p . That is, at $x/L_p = -0.05$ (before the breaking point) the energy is allocated at frequencies $f_0 - f_6$. It may be worth noting here that the majority of the higher harmonic frequency components is generated during the shoaling process, and the wave breaking provides a relatively minor contribution to the generation (Nakagawa, 1983a). At $x/L_p = 0.16$, the energies at these frequencies are decreased, and the energy at f_6 disappears. Similarly, at $x/L_p = 0.6$, the energies at $f_0 - f_4$ decrease, and the energy at f_5 disappears. Furthermore, at $x/L_p = 3.6$, the energies at $f_0 - f_2$ decrease, and the energies at f_3 and f_4 disappear. These results infer that the potential energies of the wave are transported to the higher and/or lower frequency ranges with increasing the distance x/L_p . It is evident, however, that the fundamental frequency of the original wave is preserved, even if the wave experiences the shoaling and breaking processes.

Figs. 11a, 11b and 11c show power spectra of \hat{u} , \hat{v} , and \hat{w} at $x/L_p = 0.6$ (after the breaking point) and at 2 cm below the wave trough, respectively. These figures indicate that, while the energies of \hat{u} , \hat{v} , and \hat{w} are redistributed to a wider frequency range by the shoaling and breaking, each spectrum has sharp peaks at the fundamental frequency f_0 and the first harmonic frequency f_1 . These results also suggest that, even after experiencing strong shoaling and wave breaking, the fundamental frequency of the original wave is preserved in the water particle velocities.

Figs. 12a, 12b and 12c show power spectra of \hat{u} , \hat{v} , and \hat{w} at $x/L_p = 0.6$ and at 2 cm above the horizontal bed, respectively. A

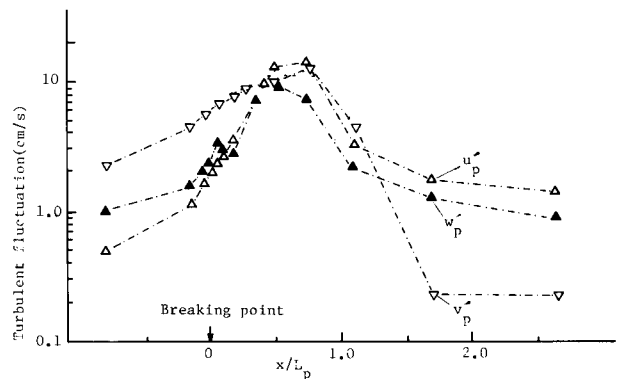


Fig. 9 Turbulent fluctuations (u' , v' , w') against distance x/L_p from the breaking point (after Nakagawa, 1983a)

comparison between Figs. 11 and 12 shows how the power spectra vary while the measurement point approaches the horizontal tank bed. That is, according to this change, the energies of \hat{u} , \hat{v} , and \hat{w} at the fundamental and higher harmonic frequencies are transported both to the lower and higher frequency ranges. As a result, each spectrum near the horizontal tank bed becomes smaller than that near the water surface.

Figs. 13a, 13b and 13c show power spectra of \hat{u} , \hat{v} , and \hat{w} at $x/L_p = 3.6$ and at 2 cm below the wave trough, respectively. Figs. 11 and 13 show that these energies at the fundamental and higher harmonic frequencies are decreased with increasing x/L_p .

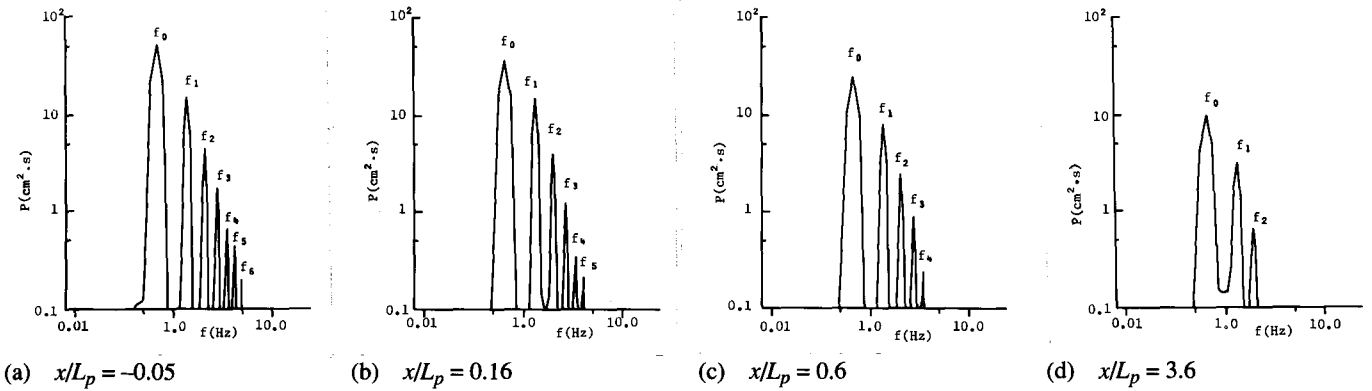
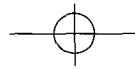


Fig. 10 Power spectra of η at various longitudinal distances

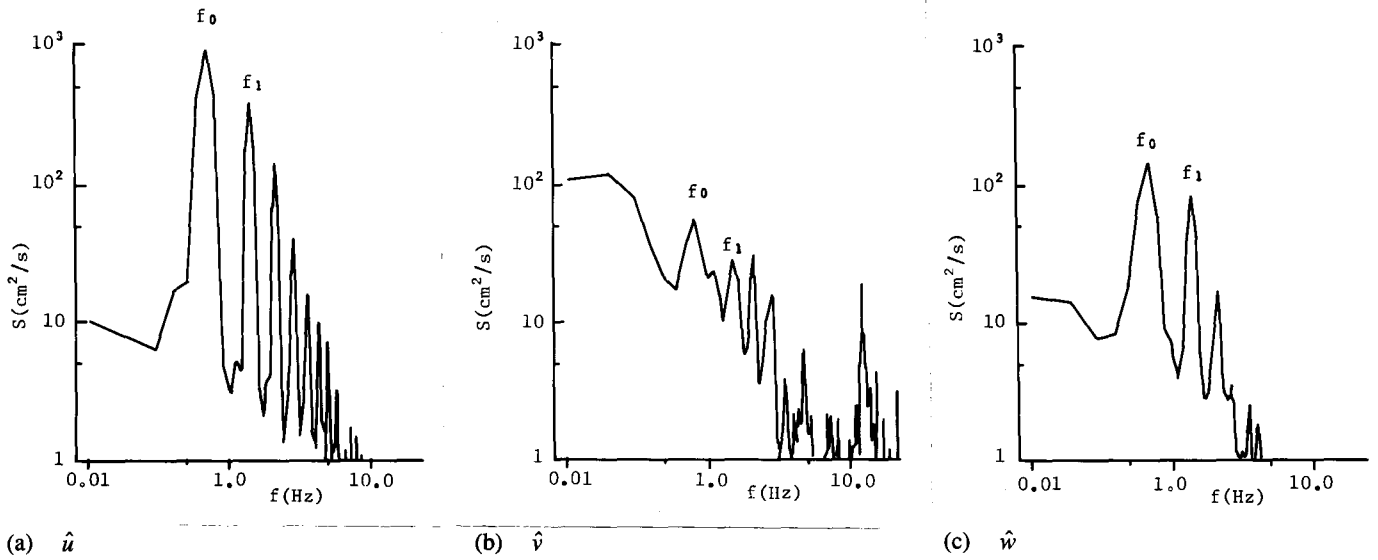


Fig. 11 Power spectra of the unsteady flows at $x/L_p = 0.6$ and at 2 cm below the wave trough

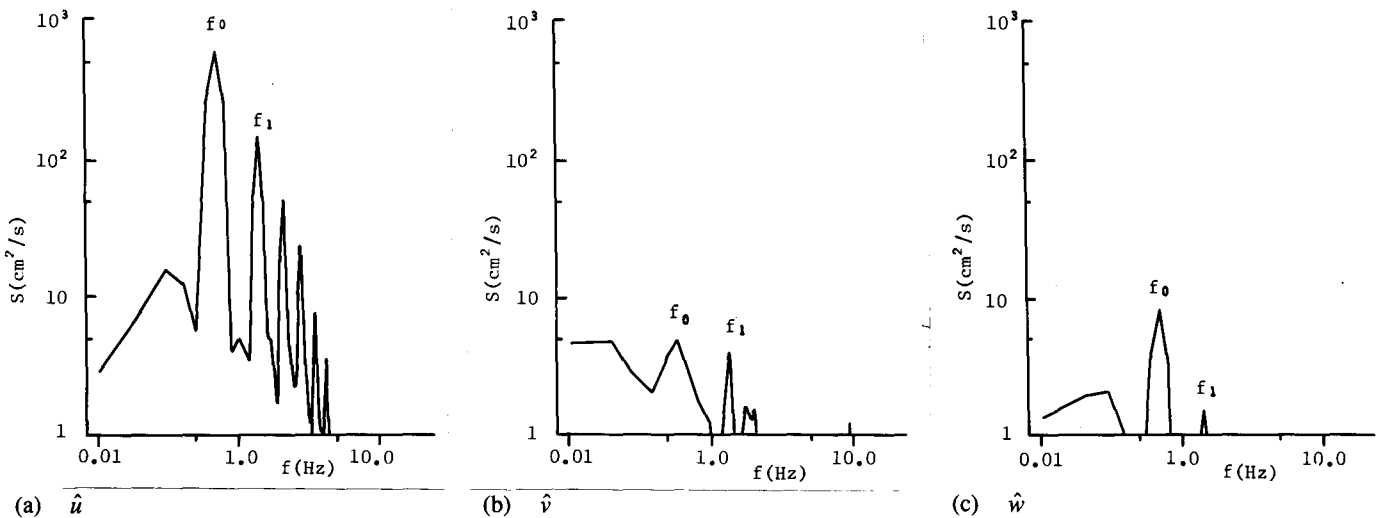


Fig. 12 Power spectra of the unsteady flows at $x/L_p = 0.6$ and at 2 cm above the horizontal bed

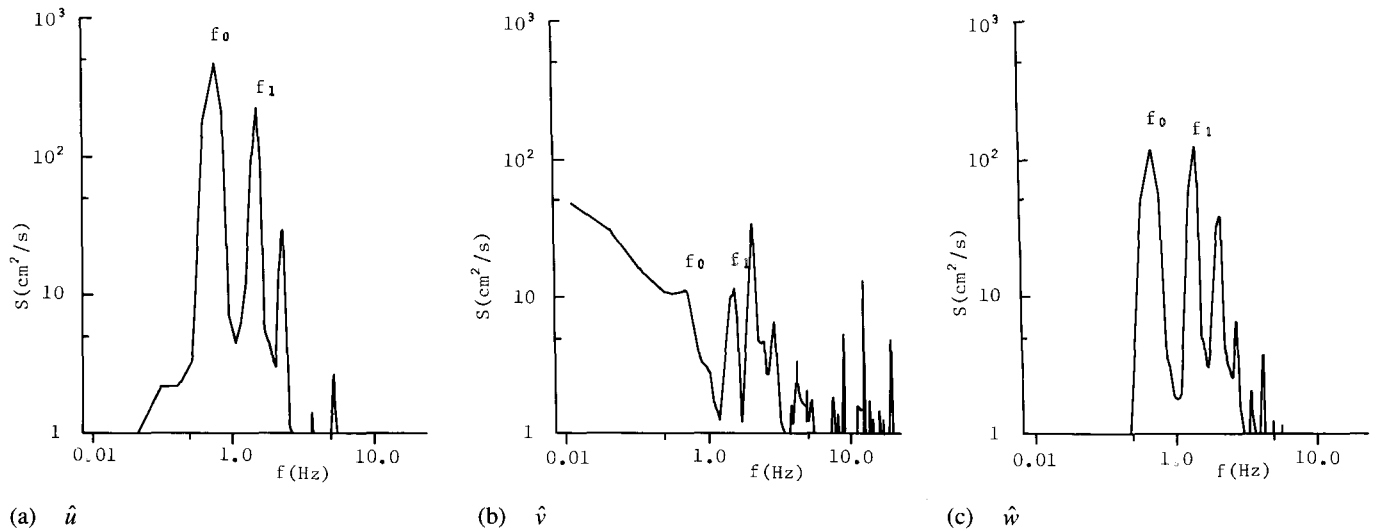


Fig. 13 Power spectra of the unsteady flows at $x/L_p = 3.6$ and at 2 cm below the wave trough

CONCLUSION

It is found that the ratio of the local wave height to the original wave height for the spilling breaker is much smaller than that for the plunging breaker, but both ratios take their maxima just before the breaking point. Note the maximum height of the spilling breaker exceeds the original value only slightly.

Before the breaking, the wave profile becomes asymmetrical through the wave shoaling process, but the wave maintains the regular oscillation with the fundamental frequency and the higher harmonics. After the breaking, the correlation between the water surface elevation and the unsteady flow component of the water particle velocity is preserved. However, the correlation decreases in approaching the tank bed and in increasing the distance from the breaking point, respectively. At each depth the correlation between the water surface elevation and the longitudinal unsteady flow component is the largest, while that between the water surface elevation and the transverse unsteady flow component is the smallest. As the wave increases the distance from the breaking point, its profile gradually changes into a symmetrical one, but the difference between the onshore and offshore velocities is increased.

After experiencing strong shoaling and breaking, the main frequencies of the original wave are preserved in the longitudinal and vertical unsteady flow components of the water particle velocity, and part of the original wave energy is transported to the transverse unsteady flow component at the same frequencies as those of the original wave. The higher harmonics in the power spectrum of the water surface profile increase through the wave shoaling process with the approach of the breaking point. However, after the breaking, they are decreased as the distance from the breaking point as well as that from the water surface increases.

ACKNOWLEDGEMENTS

The author is grateful to Mr. H. Koyama and Dr. K. Iwata for their great help in conducting the present experiment at the Department of Civil Engineering, Nagoya University, Japan, and for data analysis.

REFERENCES

- Adeymo, MD (1970). "Velocity Field in the Wave Breaker Zone," *Proc 12th Conf Coastal Eng*, pp 435-445.
- Battjes, JA (1988). "Surf-Zone Dynamics," *Ann Rev Fluid Mech*, Vol 20, pp 257-293.
- Blackman, RB, and Turkey, VW (1958). *The Measurement of Power Spectra*, Dover.
- Miller, RL, and Ziegler, JM (1964). "The Internal Velocity Field in Breaking Waves," *Proc 9th Conf Coastal Eng*, pp 103-113.
- Morison, JR, and Crooke, RC (1953). "The Mechanics of Deep Water, Shallow Water, Breaking Waves," *Tech Memo No 40*, Beach Erosion Board, Washington, D.C.
- Nadaoka, K (1986). "A Fundamental Study on Shoaling and Velocity Field Structure of Water Waves in the Near Shore Zone," *Tech Rep No 36*, Tokyo Inst Tech, Japan.
- Nakagawa, T (1983a). "On Characteristics of the Water-Particle Velocity in a Plunging Breaker," *J Fluid Mech*, Vol 126, pp 251-268.
- Nakagawa, T (1983b). "A New Instrument to Measure Three Velocity Components of Water Particles in Breaking Waves," *J Phys E: Sci Inst*, Vol 16, pp 162-163.
- Peregrine, DH (1983). "Breaking Waves on Beaches," *Ann Rev Fluid Mech*, Vol 15, pp 149-178.
- Scott, JC (1975). "The Role of Salt in White Cap Persistence," *Deep Sea Res*, Vol 22, pp 653-657.
- Svendsen, IA, Madsen, PA, and Hansen, JB (1978). "Wave Characteristics in the Surf Zone," *Proc 16th Conf Coastal Eng*, pp 520-539.
- Thornton, EB, Galvin, JJ, Bub, FL, and Richardson, DP (1976). "Kinematics of Breaking Waves," *Proc 15th Conf Coastal Eng*, pp 461-471.
- Walker, JR (1969). "Estimation of Ocean Wave-Induced Particle Velocities from the Time History of a Bottom Mounted Pressure Transducer," *M Sc Thesis*, Univ Hawaii, USA.
- Wood, WL (1973). "A Wave and Current Investigation on the Near Shore Zone," *Mich State Univ*, USA.